ADVANCES IN ATMOSPHERIC SCIENCES, VOL. 31, SEPTEMBER 2014, 1209–1220

Analyses of Extreme Climate Events over China Based on CMIP5 Historical and Future Simulations

YANG Shili[1], FENG Jinming*[2,3], DONG Wenjie[1], and CHOU Jieming[1]

[1]*State Key Laboratory of Earth Surface Process and Resource Ecology, Beijing Normal University, Beijing* 100875
[2]*Key Laboratory of Regional Climate–Environment for East Asia, Institute of Atmospheric Physics, Chinese Academy of Sciences, Beijing* 100029
[3]*College of Global Change and Earth System Science, Beijing Normal University, Beijing* 100875

(Received 7 June 2013; revised 10 December 2013; accepted 10 January 2014)

ABSTRACT

Based on observations and 12 simulations from Coupled Model Intercomparison Project Phase 5 (CMIP5) models, climatic extremes and their changes over China in the past and under the future scenarios of three Representative Concentration Pathways (RCPs) are analyzed. In observations, frost days (FD) and low-temperature threshold days (TN10P) show a decreasing trend, and summer days (SU), high-temperature threshold days (TX90P), heavy precipitation days (R20), and the contribution of heavy precipitation days (P95T) show an increasing trend. Most models are able to simulate the main characteristics of most extreme indices. In particular, the mean FD and TX90P are reproduced the best, and the basic trends of FD, TN10P, SU and TX90P are represented. For the FD and SU indexes, most models show good ability in capturing the spatial differences between the mean state of the periods 1986–2005 and 1961–80; however, for other indices, the simulation abilities for spatial disparity are less satisfactory and need to be improved. Under the high emissions scenario of RCP8.5, the century-scale linear changes of the multi-model ensemble (MME) for FD, SU, TN10P, TX90P, R20 and P95T are −46.9, 46.0, −27.1, 175.4, and 2.9 days, and 9.9%, respectively; and the spatial change scope for each index is consistent with the emissions intensity. Due to the complexities of physical process parameterizations and the limitation of forcing data, great uncertainty still exists with respect to the simulation of climatic extremes.

Key words: extreme climate, China, CMIP5, RCPs

Citation: Yang, S. L., J. M. Feng, W. J. Dong, and J. M. Chou, 2014: Analyses of extreme climate events over China based on CMIP5 historical and future simulations. *Adv. Atmos. Sci.*, **31**(5), 1209–1220, doi: 10.1007/s00376-014-3119-2.

1. Introduction

Changes in climatic extremes have more serious impacts on human society, the economy and ecosystems compared to mean climate changes (Meehl et al., 2000). Great efforts have been made to understand the physical mechanisms and evolution of changes in climatic extremes under the global warming background. In recent years, extensive research has been conducted on the spatial distribution and temporal evolution of extreme temperature and precipitation over China using various statistical methods (Jiang et al., 1999; Zhai et al., 1999; Yan and Yang, 2000; Zhai and Pan, 2003; Zhai et al., 2005; Chen et al., 2009; Ren et al., 2010). Zhai et al. (1999) used monthly observations of 369 stations to focus mainly on the annual and seasonal changes, while Zhai et al. (2005) used daily data of 740 stations to focus mainly on the spatial distribution. Comprehensively, these studies have mostly illustrated that both the annual average maximum and minimum temperature show increasing trends over the whole of China, while the most significant warming tendency is found over North China, with the largest warming amplitude in winter. Furthermore, the frequency of extreme precipitation events has also increased. Ren et al. (2010) used an extreme climate index to reveal a decrease in extreme events related to anomalous cold conditions (e.g. frost days), and an increase in extreme events related to anomalous warm conditions (e.g. warming days). Based on the above-mentioned investigations, coupled climate models have been used to explore future climate change scenarios with a focus on climatic extremes (Gao et al., 2002; Jiang et al., 2004; Jiang et al., 2007; Zhang et al., 2007; Jiang et al., 2012; Wang et al., 2012; Lang and Sui, 2013). Jiang et al. (2012) evaluated and projected some extreme indices over China using Coupled Model Intercomparison Project Phase 3 (CMIP3) models. Their results showed that the global coupled climate models that they studied have the ability to reproduce the spatial distribution and linear trends of the extreme indices, and that the extreme precipitation index tends to increase in the 21st century.

* Corresponding author: FENG Jinming
Email: fengjm@tea.ac.cn

Important progress has been made through the development of global coupled models and climate simulations. The outputs of tens of models' historical experiments and future projections of the different Representative Concentration Pathways (RCPs) are being supplied as part of the Coupled Model Intercomparison Project Phase 5 (CMIP5). These outputs provide a good opportunity to evaluate the capacity of coupled models in simulating extreme climate events over China, as well as project their future changes. In the present paper, the performances of CMIP3 models are also referenced and discussed, giving us greater confidence in terms of the future projections of extreme climate change based on CMIP5 outputs.

The remainder of the paper is organized as follows. First, the observations, CMIP5 model datasets, extreme indices, and methods used in the study are described in section 2. In section 3, model performances are validated by comparing CMIP5 outputs with observations. Mean climate, temporal evolution, and spatial distribution of six extreme indices are considered in this study. CMIP5 results for 2006–99 are employed to project the changes in extreme climate under future scenarios. Finally, a summary and discussion of the key findings are given in section 4.

2. Datasets, extreme indices, and methodology

2.1. *Datasets*

The observations used to validate the simulation results are $0.5^\circ \times 0.5^\circ$ gridded daily maximum temperature (TX), minimum temperature (TN), and precipitation (PRCT) over China (Xie et al., 2007; Xu et al., 2009). The dataset covers the period 1961–2005.

The coupled climate model outputs are taken from the CMIP5 multi-model data archive (http://cmip-pcmdi.llnl.gov/cmip5/index.html). In the study, the main focus is on the 20th century historical experiments, and the projection experiments under the RCP2.6, RCP4.5 and RCP8.5 scenarios. In total, the outputs of 12 models are employed. As we know, greenhouse gas emissions are the main cause of current global warming. In order to better understand global change, especially with respect to extreme climate, the changes in carbon dioxide (CO_2) and sulfate aerosol (SO_4) concentrations in the past and future (under different RCPs) are presented in Fig. 1. The data show a clear increase in the CO_2 concentration both in the past and in the future; while the historical SO_4 concentration in China shows an increasing trend, and a future peak appears at around 2020–40, before decreasing to the level of the mid-20th century by the year 2100. Table 1 provides detailed descriptions of the models examined in this study. In order to facilitate the comparison of model results with observations, the bilinear interpolation method is used to re-grid the model outputs to $0.5^\circ \times 0.5^\circ$ grids, i.e. to bring them in line with observations.

2.2. *Extreme indices*

The World Meteorological Organization (WMO) provides more than 30 extreme indices (Karl et al., 1999), and considers China to be easily influenced by extreme events related to minimum/maximum temperature and heavy rain. For

Table 1. Model descriptions.

Model	Model Expansions	Institution	Resolution (lat×lon)	References
BCC-CSM	Beijing Climate Center Climate System Model	Beijing Climate Center	$2.8^\circ \times 2.8^\circ$	Wu et al. (2010)
BNU-ESM	Beijing Normal University Earth System Model	Beijing Normal University	$2.8^\circ \times 2.8^\circ$	Wu et al. (2013)
CanCM4	Canadian Centre for Climate Modeling and Analysis Coupled Climate Model Version 4	Canadian Centre for Climate Modeling and Analysis	$2.8^\circ \times 2.8^\circ$	Flato et al. (2000)
CanESM2	Version 2 of Canadian Earth System Model	Canadian Centre for Climate Modeling and Analysis	$2.8^\circ \times 2.8^\circ$	Gillett et al. (2012)
CCSM4	Version 4 of Community Climate System Model	National Center for Atmospheric Research	$0.9^\circ \times 1.25^\circ$	Gent et al. (2011)
CNRM-CM5	Institute Pierre Simon Laplace Climate Model Version 5	Centre National de Recherches Meteorologiques	$1.4^\circ \times 1.4^\circ$	Voldoire et al. (2011)
GFDL-ESM2M	Geophysical Fluid Dynamics Laboratory Earth System Model	Geophysical Fluid Dynamics Laboratory	$2.0^\circ \times 2.5^\circ$	Dunne et al. (2012)
GISS-E2-R	Goddard Institute for Space Studies Model E with Russell Ocean Model	Goddard Institute for Space Studies	$2.0^\circ \times 2.5^\circ$	Hansen et al. (1983)
HadCM3	Hadley Center Model Version 3	Hadley Centre for Climate Research	$3.8^\circ \times 2.5^\circ$	Collins et al. (2001)
IPSL-CM5A	Institute Pierre Simon Laplace Climate Model Version 5	Institut Pierre Simon Laplace	$1.9^\circ \times 3.8^\circ$	Marti et al. (2010)
MIROC-ESM	Japan Agency for Marine-Earth Science and Technology Earth System Model	Japan Agency for Marine-Earth Science and Technology	$2.8^\circ \times 2.8^\circ$	Watanabe et al. (2011)
MRI-CGCM3	Meteorological Research Institute Coupled General Circulation Model version 3	Meteorological Research Institute	$1.1^\circ \times 1.1^\circ$	Yukimoto and Noda (2002)

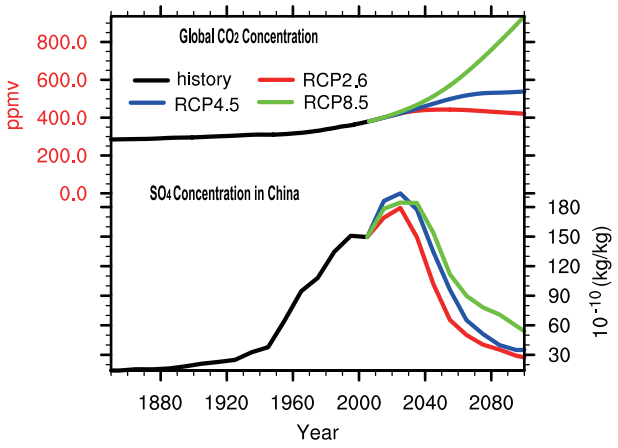

Fig. 1. Historical and future (under RCP scenarios) changes of CO_2 and SO_4 concentrations over China.

example, heat waves can occur in summer, often resulting in heat stroke or, in the worst-case scenario, death; while frost can cause significant losses and disruption for agriculture and transport, and heavy rain can cause floods. For this paper, we selected four representative extreme temperature indices and two representative extreme precipitation indices defined by the WMO. Details regarding these extreme indices are given in Table 2.

The six extreme indices consist of three defined by absolute threshold (FD, SU and R20), and three defined by percentage threshold (TN10P, TX90P and P95T), which together reflect the different perspectives of extreme climate events. The chosen indices have been widely investigated in the past through both observational and model simulation studies, which provide useful information on understanding whether the CMIP5 models have improved in terms of their simulate and project skill.

2.3. *Methodology*

The methods used to calculate the extreme indices defined by the percentage threshold are as follows. For the TN10P and TX90P indexes: sort the daily data on the same day of all years from the baseline period (1961–90) into ascending order; determine the percentile value; then calculate the number of days of each year whose value is greater (for TX90P) or smaller (for TN10P) than the corresponding percentile value. For the P95T index: sort the precipitation on wet days (> 1.0 mm) into ascending order in the same year; determine the 95% percentile value; then obtain the average 95% percentile value in the baseline period (1961–90); and finally, calculate the contribution of annual total precipitation that exceeds the average 95% percentile value.

The multi-model ensemble (MME) mean is calculated using the arithmetic mean, i.e., each model has the same weight. The model relative error (E) is expressed as:

$$E_{i,j} = \frac{M_{i,j} - O_j}{O_j} \times 100\% \,,$$

where $E_{i,j}$ represents the relative error of the ith model for the jth index; $M_{i,j}$ represents the ith model result for jth index; and O_j represents the observed jth index.

Non-parametric Mann-Kendal (MK) statistics (Mann, 1945; Kendall, 1948) were used to test linear trends.

3. Results

3.1. *Mean values*

Figure 2 shows the results of model simulations versus observations for the regional and yearly averages of the six extreme indices over the whole of China during 1961–2005. As can be seen, the ability to simulate the indices differs among the various models. In general, the characteristics of the FD index are best represented by the models. Compared to observations, the E of the FD and TX90P indexes for a single model are in the range -7.6%–13.9% and -5%–5%, respectively. However, they are only 1.7% and -1.0% for the MME, which reflects the superiority of using the MME compared to any single model. All the models underestimate the SU index (Fig. 2b) but overestimate the TN10P index (Fig. 2c), and the corresponding E of the MME reach -28.8% and 12.9%, respectively. This result indicates that the majority of the models underestimate both the absolute extreme maximum temperature and the threshold extreme minimum temperature. Most of the models also underestimate the precipitation index, R20 (Fig. 2e), which is consistent with CMIP3 results (Jiang et al., 2009). Despite the fact that most models produce lower R20 index, their E are very small. The E for the MME of R20 is only -3.8%, indicating that the disparity is not too great, although the frequency of extreme precipitation is underestimated. The E of the P95T index for a single model is in the range -12.7%–11%, but for the MME it is only 0.3%.

The magnitude of the absolute value of E is used as an indication of a model's performance relative to other models.

Table 2. Extreme index definitions.

Index name	Definition	Units
Frost days (FD)	Total number of days when TN $< 0^\circ$C	d
Summer days (SU)	Total number of days when TX $> 25^\circ$C	d
Low-temperature threshold days (TN10P)	Percentage of days when TN $<$ 10th percentile	d
High-temperature threshold days (TX90P)	Percentage of days when TX $>$ 90th percentile	d
Heavy precipitation days (R20)	Total number of days when PRCT $>$ 20 mm	d
Heavy precipitation contribution (P95T)	The contribution of annual total precipitation when PRCT $>$ 95th percentile	%

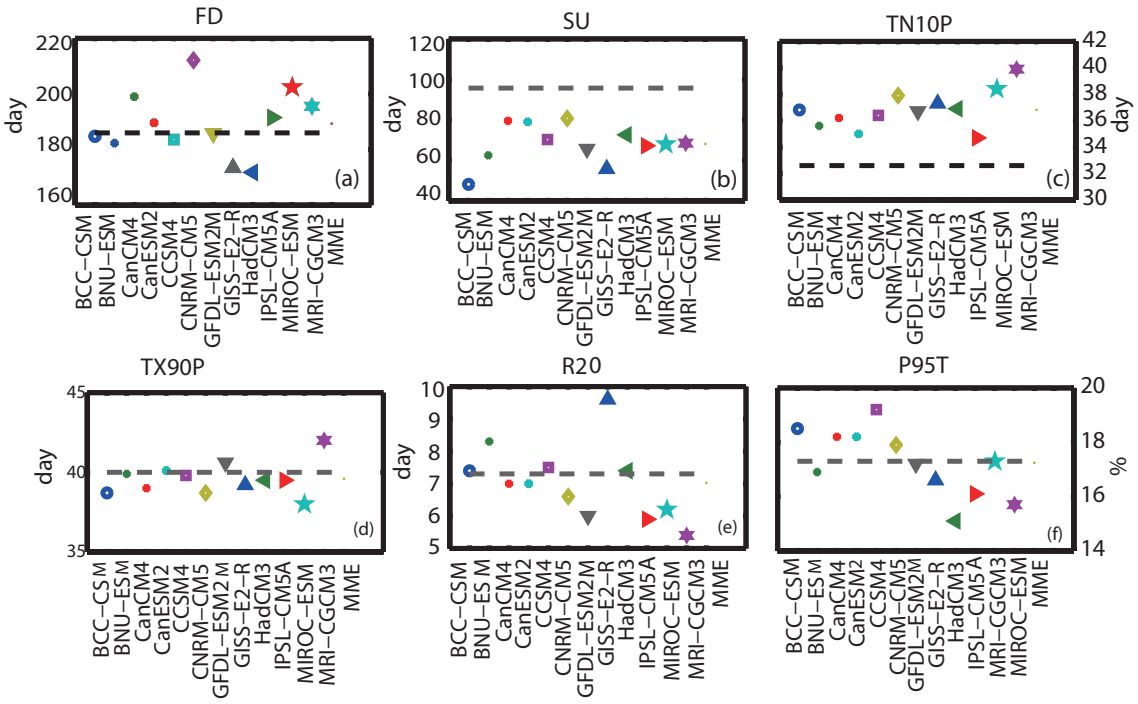

Fig. 2. Observed and modeled multi-year average for each index (dashed line: observation).

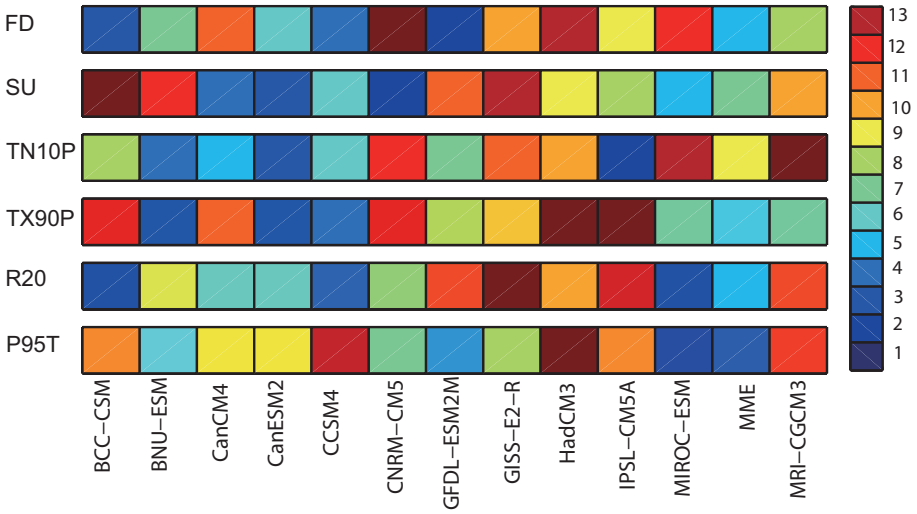

Fig. 3. Model simulation skill denoted by relative error order for each index.

Figure 3 shows the skill of the models in simulating the six extreme climate indices. Their skill levels are ordered from 1 to 13 for each index. For each model, the lower the order number, the higher its simulation skill. From Fig. 3 it can be seen that CanESM2 performs best, with five indices (all apart from P95T) ranking in the top six among the 12 models. Five indices (again, all apart from P95T) of CCSM4 also rank in the top six, while four indices (all apart from FD and TN10P) of MIROC-ESM rank in the top six. MIROC-ESM has the best ability to simulate the extreme precipitation index. Overall, it appears that CCSM4, CanESM2 and MIROC-ESM have the highest capabilities in reproducing the mean index values. Figure 3 also indicates that the MME improves the skill to some extent, but it definitely relies on the capability of each single model.

3.2. *Temporal evolution*

To compare the temporal evolution of modeled and observed indices, linear trends are calculated using the least-squares method and trend significance is assessed using the MK test at the 5% level. In addition, the time series for each of the six indices are presented to evaluate and compare the models' abilities in reproducing the temporal evolution. The linear trends and associated significance are given in Table 3.

Table 3. Observed and simulated decadal trend for each index [units: (10 yr)$^{-1}$]. Bold type indicates the trend is significant at the 5% level; values in parentheses are the standard deviation of the models for each index.

Model	Index					
	FD	SU	TN10P	TX90P	R20	P95T
BCC-CSM	**−2.0**	**1.3**	**1.3**	**3.2**	−0.04	0.22
BNU-ESM	**−2.6**	**2.5**	**−3.4**	**4.5**	−0.10	**0.62**
CanCM4	**−2.1**	**2.0**	**−1.4**	**3.7**	**0.13**	0.29
CanESM2	**−3.0**	**2.7**	**−3.1**	**4.4**	0.09	0.23
CCSM4	**−2.3**	**2.0**	**−2.6**	**4.8**	−0.03	0.22
CNRM-CM5	**−1.3**	0.6	0.4	**2.4**	**0.20**	**0.67**
GFDL-ESM2M	**−2.3**	**2.7**	−0.3	**4.8**	0.01	**0.44**
GISS-E2-R	**−1.5**	0.6	−0.5	**3.2**	−0.04	0.17
HadCM3	**−1.7**	**1.5**	−0.1	**2.7**	−0.05	0.32
IPSL-CM5A	**−2.8**	**2.6**	**−4.0**	**7.2**	0.07	**0.35**
MIROC-ESM	**−1.1**	−0.2	**1.5**	**3.2**	0.22	**0.28**
MRI-CGCM3	**−1.5**	0.6	1.5	**4.5**	−0.07	0.09
MME	**−2.0** (0.6)	**1.6** (1.0)	**−1.1** (1.9)	**4.1** (1.3)	0.04 (0.1)	**0.33** (0.2)
OBS	**−3.1**	**1.8**	**−2.8**	**2.4**	0.01	**0.33**

It is clear that the observed FD and TN10P show significant decreasing trends, while the SU and TX90P index have increasing trends. However, little change is found for R20 and P95T. Furthermore, these regional trend characteristics are similar to those found at the global scale (Alexander et al., 2006; Sillmann et al., 2013a). The models can basically reproduce the time evolution of the extreme indices, especially for FD, SU, TN10P and TX90P (Fig. 4). A significant decreasing trend of the FD index is found in all model results, but the magnitude is less than that in the observation [−3.1 d (10 yr)$^{-1}$]. The FD trend across the models' results falls in the range −3.0 to −1.1 d (10 yr)$^{-1}$, while that of the MME is −2.0 d (10 yr)$^{-1}$. Apart from MIROC-ESM, the other 11 models are able to reproduce the trend of the SU index in the same direction as the observed trend. These simulated trends, as well as the MME trend, are statistically significant, except for those of CNRM-CM5, GISS-E2-R and MRI-CGCM3. The SU trend in the observation and MME result is 1.6 and 1.8 d (10 yr)$^{-1}$, respectively. Apart from CNRM-CM5, MIROC-ESM and MRI-CGCM3, the other nine models agree with the observed decreasing trend of the TN10P index. The simulated decreasing trend of TN10P is statistically significant for most of the models. The TN10P trend in the observation and MME result is −1.1 and −2.8 d (10 yr)$^{-1}$, respectively. All the models are able to reproduce the significant increasing trend of TX90P, but overestimate the trend magnitude. The TX90P trend in the observation is 2.4 d (10 yr)$^{-1}$, while that of the MME is 4.1 d (10 yr)$^{-1}$.

The observed trends of the extreme precipitation indices are very small, and they are not statistically significant, especially for R20. CanCM3, CNRM-CM5 and MIROC-

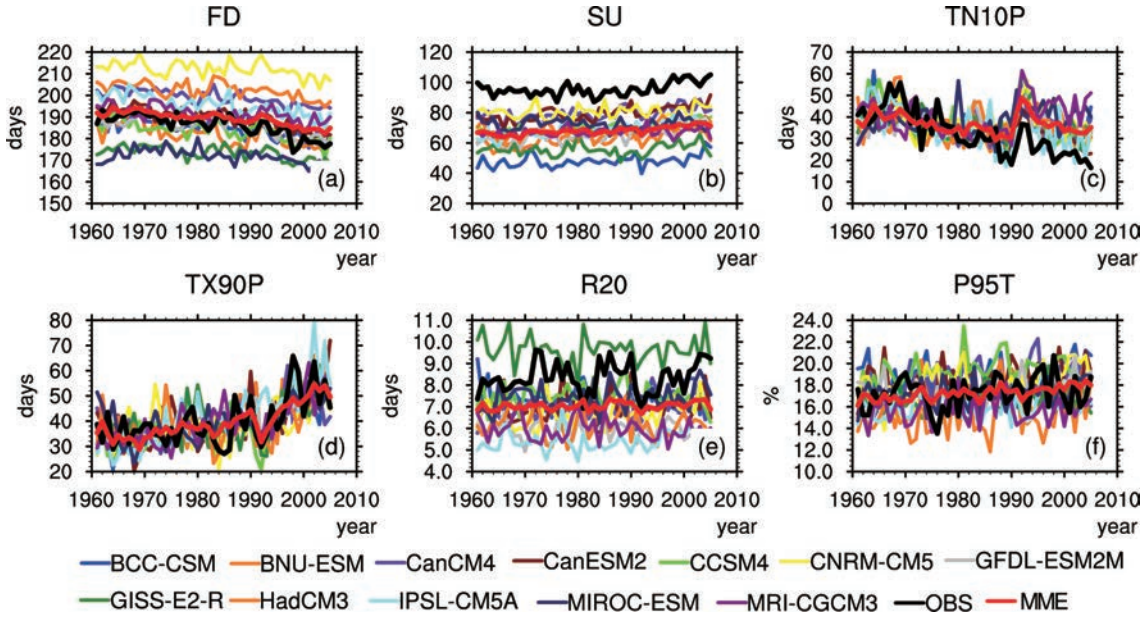

Fig. 4. Observed and modeled time series of each extreme index.

ESM overestimate the linear trend of R20, while BNU-ESM, CCSM4, HadCM3 and MRI-CGCM3 models give an opposite trend. The models are in agreement with the observation for the P95T trend.

Therefore, the models are able to simulate extreme temperature indices better than extreme precipitation indices. In addition, most of the models are generally able to reproduce the temporal evolution and linear trend within a reasonable range.

3.3. *Spatial distribution*

The spatial correlation between observed and modeled extreme indices is calculated to quantify their similarity. Before calculating the correlation, the temporal average from 1961 to 2005 is first obtained for the six extreme indices. Figure 5 shows that there are great differences in spatial correlation among the different indices. Overall, the top three indices with high correlation coefficients are FD, SU, and P95T. Their correlation exceeds 0.85, 0.6 and 0.5, respectively. Correlations of the TN10P and TX90P indexes are lower, and large dispersion exists among the different models. The results are not statistically significant for most models, and the correlations of many of the models are even negative.

The spatial distribution of climatic extreme change can be reflected by comparing the observed and modeled spatial disparity between the last two decades (1986–2005) and the first two decades (1961–80) of the historical period. Figure 6 indicates an observed decrease of the FD index in most regions of China, especially the northeast. Apart from CanCM4, MIROC-ESM and CNRM-CM5, the models are able to capture this characteristic, but with smaller change amplitude. The shortcoming of the models is that the majority of them (except BNU-ESM, CanCM4 and CanESM2) show an increase in southern China, which did not happen according to observations. The observed SU index changes show a smaller spatial difference, and with amplitude in the range 0–6 days. The BCC-CSM, CCSM4, GFDL-ESM2M, HadCM3 and MRI-CGCM3 models, as well as the MME, show good performance, while BNU-ESM, CanESM2 and IPSL-CM5A overestimate the changes in Northeast China (not shown). The observed TN10P and TX90P share the same regional variation characteristics in that the changes in North China are much larger than those in South China, and CanESM2 and GFDL-ESM2M show good performance in reproducing this phenomenon. The BNU-ESM, CNRM-CM5, GFDL-ESM2M, GISS-E2-R, HadCM3 and MIROC-ESM models magnify the amplitude of increase for the TN10P index across the whole of China (not shown).

There are few and uniform changes across the whole of China for the observed R20 index, but the models reflect a larger spatial difference (Fig. 7). For example, the CNRM-CM5, GFDL-ESM2M and HadCM3 models overestimate the amplitude of decrease in the R20 index over Northeast China and South China (Fig. 7). Furthermore, most of the model results show significant regional variation for the P95T index (e.g. GFDL-ESM2M and CanCM4 show visible variation centered in Northeast China), which does not reflect the observational results (not shown).

Therefore, it is relatively easy for the models to capture the temporal average value for the FD and TX90P indexes, and the MME is able to reduce the uncertainty, especially for indices related to precipitation. The models are able to not only reproduce the linear trend in the same direction as the observation for the FD, SU, TN10P and TX90P indices, but can also reflect the spatial distribution well for the FD, SU and P95T indices. The model results regarding the spatial difference between the first and last two decades of the historical period (1986–2005 and 1961–80) are different among the models for various indices. For the FD and SU indexes, most of the models' results (all apart from MIROC-ESM) are consistent with the observed pattern. CanESM2 and GFDL-ESM2M show a comparative advantage in reproducing the

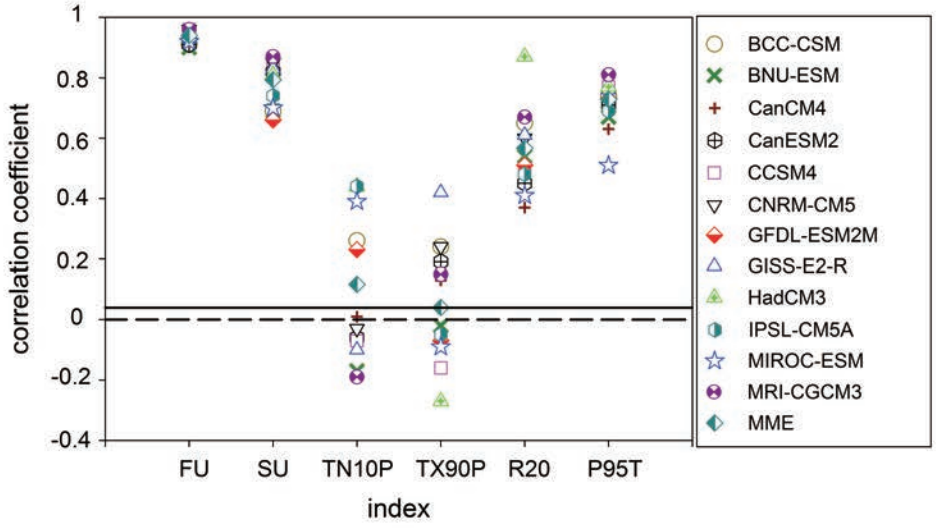

Fig. 5. Spatial correlation coefficients between observed and modeled indices (solid black line: critical value with 0.05 significance levels).

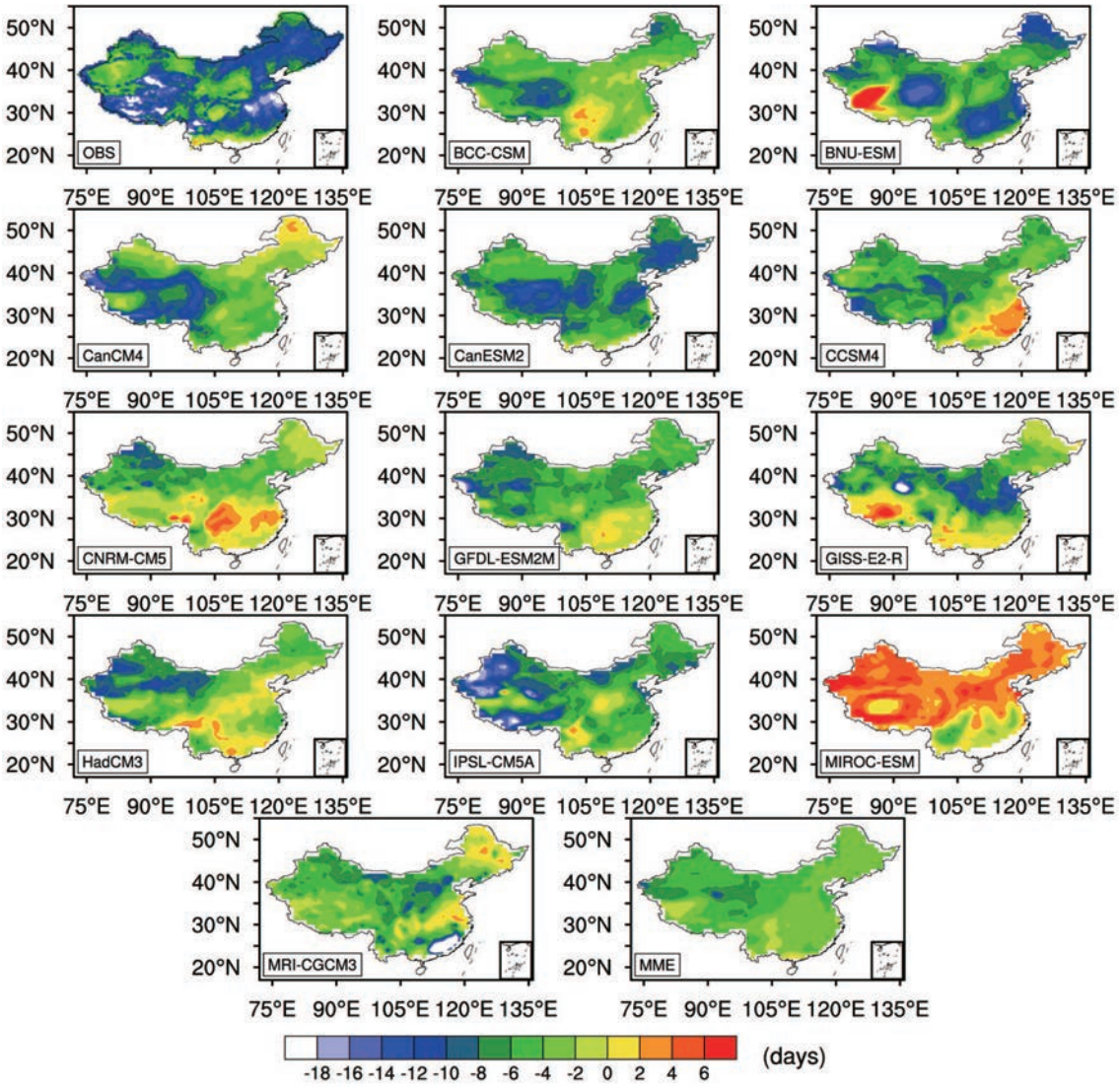

Fig. 6. Spatial distribution of the observed and modeled FD index change (averaged during 1986–2005 relative to 1961–80).

TN10P and TX90P spatial difference between the two periods. Generally speaking, each model has its own advantages and disadvantages, and there is no perfect model for reproducing all the six extreme indices. However, relatively speaking, the CCSM4 and CanESM2 models perform best according to this study.

3.4. *Future projection*

The future projection datasets for CanCM4 and HadCM3 only cover the period 2006–35. Furthermore, GISS-E2-R provides data for RCP4.5 only. Considering these data limitations, we use the other nine models (i.e. BCC-CSM, BNU-ESM, CCSM4, CanESM2, GFDL-ESM2M, IPSL-CM5A, CNRM-CM5, MIROC-ESM and MRI-CGCM3) to project future changes of extreme climate. Figure 8 shows the changes in extreme climate indices of the MME from 2006 to 2099 under RCP2.6, RCP4.5 and RCP8.5.

The extreme indexes based on minimum temperature (FD and TN10P) show a decrease, while the indexes based on maximum temperature (SU and TX90P), and precipitation (R20 and P95T), show an increase in the future, all of which are consistent with projections at the global scale (Sillmann et al., 2013b). Obviously, the trend of TX90P is the largest. Figure 8 also reveals that future trends of the extreme indices range widely under different RCPs. Obviously, under the high emissions scenario of RCP8.5, linear trends are the largest. The trend difference between RCP4.5 and RCP2.6 is relatively small.

The changes in FD, SU, TN10P, TX90P, R20 and P95T based on the MME under the low emissions scenario of RCP2.6 are -4.6, 5.1, -5.7, 17.5 and 0.6 d (100 yr)$^{-1}$, and 1.4% (100 yr)$^{-1}$, respectively. Meanwhile, those under RCP8.5 are -46.9, 46.0, -27.1, 175.4, and 2.9 d (100 yr)$^{-1}$, and 9.9% (100 yr)$^{-1}$, respectively (Table 4). For FD and TX90P, the changes under RCP8.5 are almost ten times those under RCP2.6, indicating that the risk of extreme climate increases markedly under a high emissions scenario. Under RCP8.5, the models produce changes of FD, SU, TN10P,

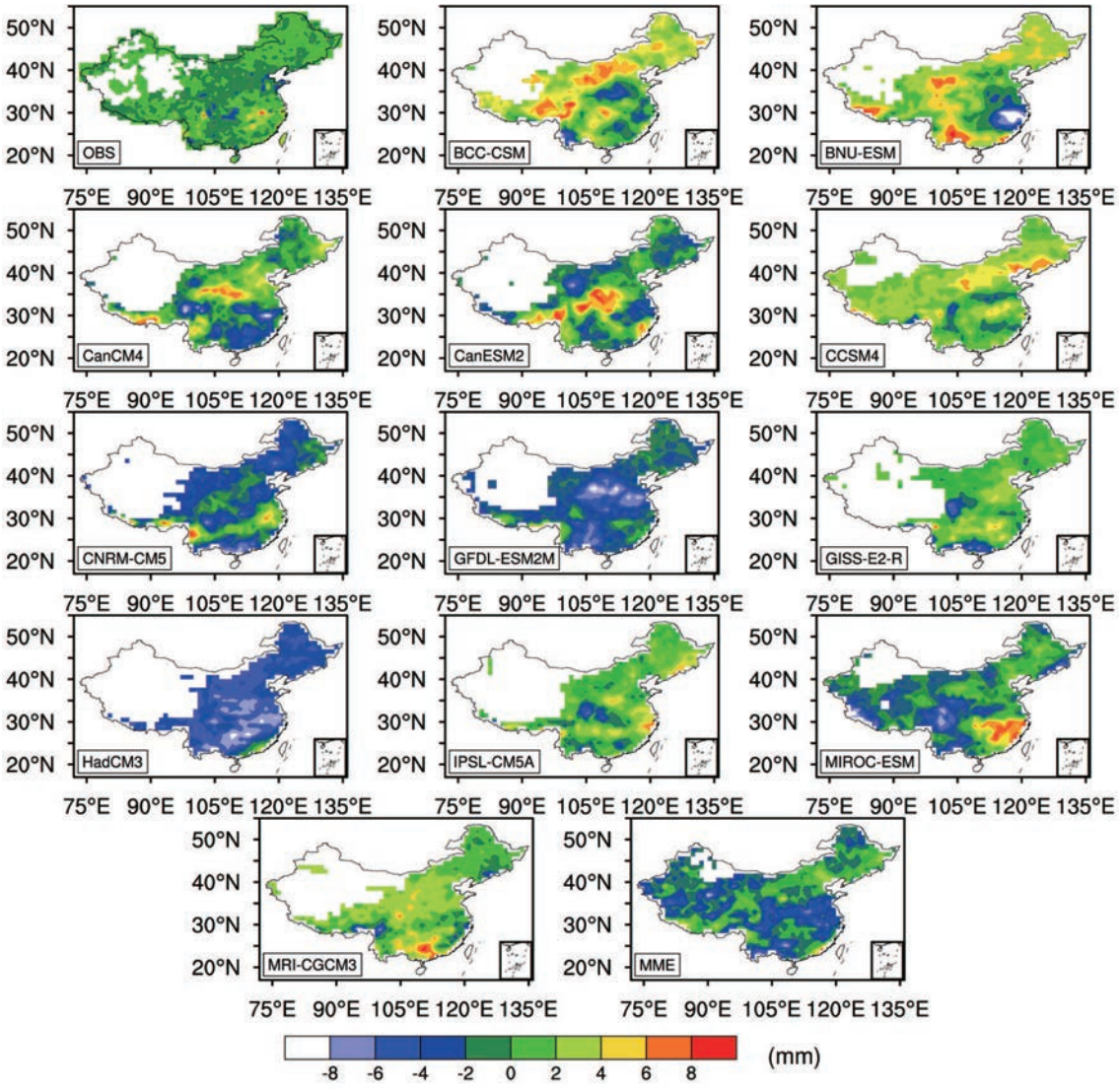

Fig. 7. The same as Fig. 6, but for R20 index.

Table 4. Linear trends of the extreme indices during 2006–99 under RCP8.5 [units: (100 yr)$^{-1}$]. Values in parentheses are the standard deviation of the models for each index.

	Index					
Model	FD	SU	TN10P	TX90P	R20	P95T
BCC-CSM	−45.5	45.5	−28.8	155.5	2.2	9.2
BNU-ESM	−49.0	54.0	−26.4	198.1	3.5	8.8
CanESM2	−56.7	50.2	−22.5	215.1	3.9	10.3
CCSM4	−42.1	42.9	−27.1	178.7	2.2	7.6
CNRM-CM5	−40.9	33.1	−14.7	149.0	1.0	5.8
GFDL-ESM2M	−36.0	37.6	−30.4	129.6	1.9	9.0
IPSL-CM5A	−57.7	61.0	−26.0	266.7	1.1	9.4
MIROC-ESM	−61.4	62.2	−23.4	278.7	2.3	9.4
MRI_CGCM3	−43.2	33.2	−38.4	158.6	1.4	8.7
MME	−48.0 (8.7)	45.7 (11.0)	−25.0 (6.3)	192.2 (59.4)	1.8 (1.0)	8.7 (1.3)

TX90P, R20 and P95T in the ranges of −56.7 to −36.0, 37.6–54.2, −30.4 to −22.5, 129.6–215.1, and 1.9–3.9 d (100 yr)$^{-1}$, and 9.2%–11.2% (100 yr)$^{-1}$, respectively. It can be seen that the degree of dispersion among the models in terms of their prediction of extreme indices in the future is not large.

Next, we use the spatial disparity between the periods 2080–99 and 1961–80 to represent the spatial changes under each scenario of each index. The results show a decrease

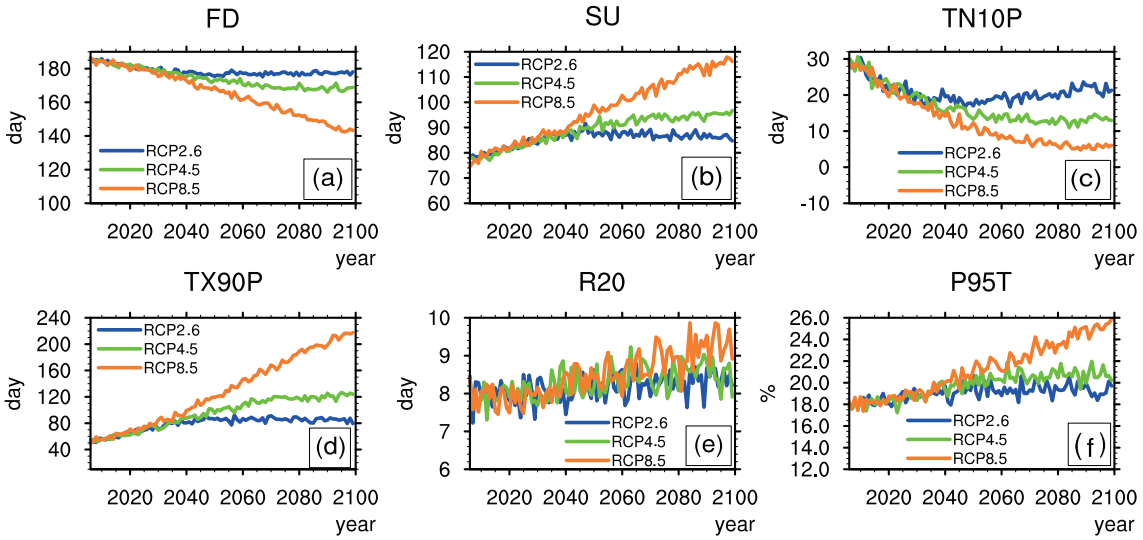

Fig. 8. Projected (2006–99) annual time series of each index based on the MME under RCP2.6, RCP4.5, and RCP8.5.

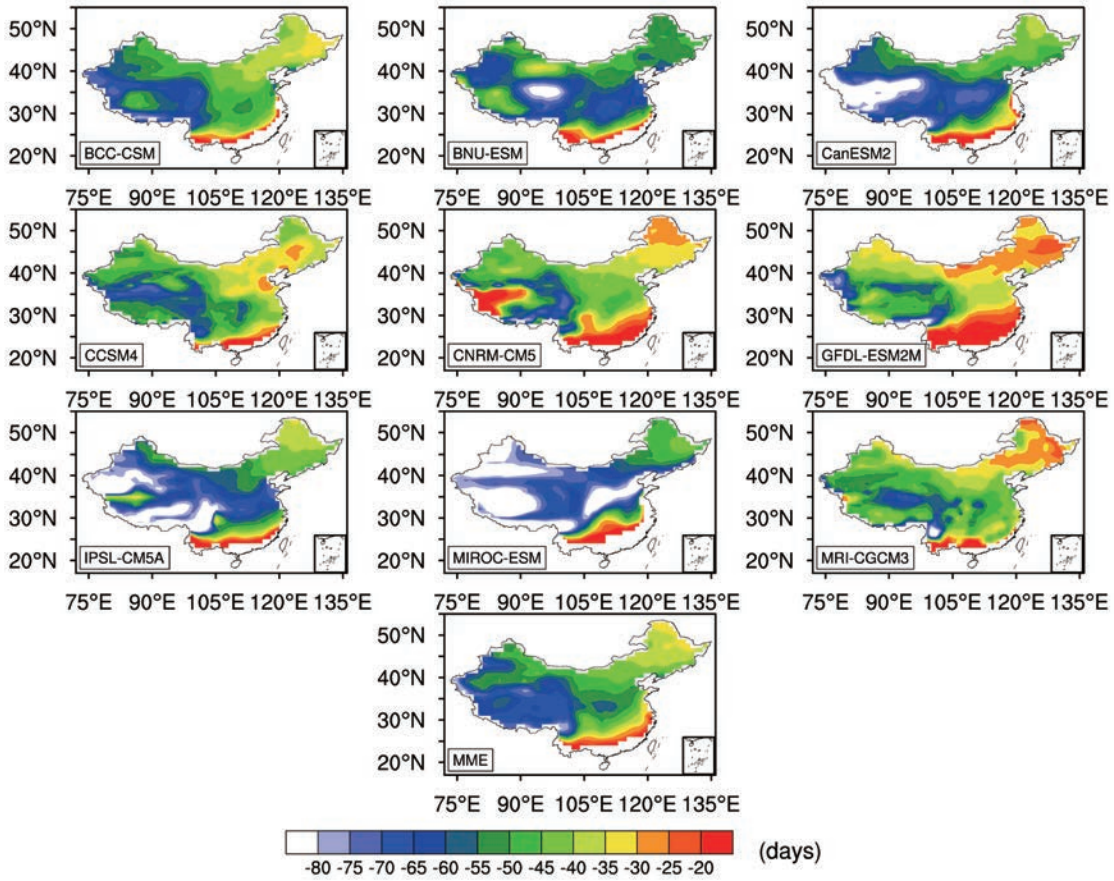

Fig. 9. Relative spatial changes of FD index under RCP8.5 (averaged for 2080–99 relative to 1961–80).

in the FD index across China under the three RCPs and, despite the magnitude of decrease in certain regions showing large differences among the models, the pattern is similar, with smaller changes in the northeast and south and larger changes in the center of China. These characteristics are particularly evident under the RCP8.5 scenario (see Fig. 9). Smaller changes in the SU index are found in Northeast China for most of the models (all apart from CanESM2 and IPSL-CM5A) under the three RCPs; and, apart from BNU-ESM and IPSL-CM5A, the models show smaller changes in the north of Xinjiang (not shown). For the TN10P and TX90P indexes, patterns among the models show larger differences.

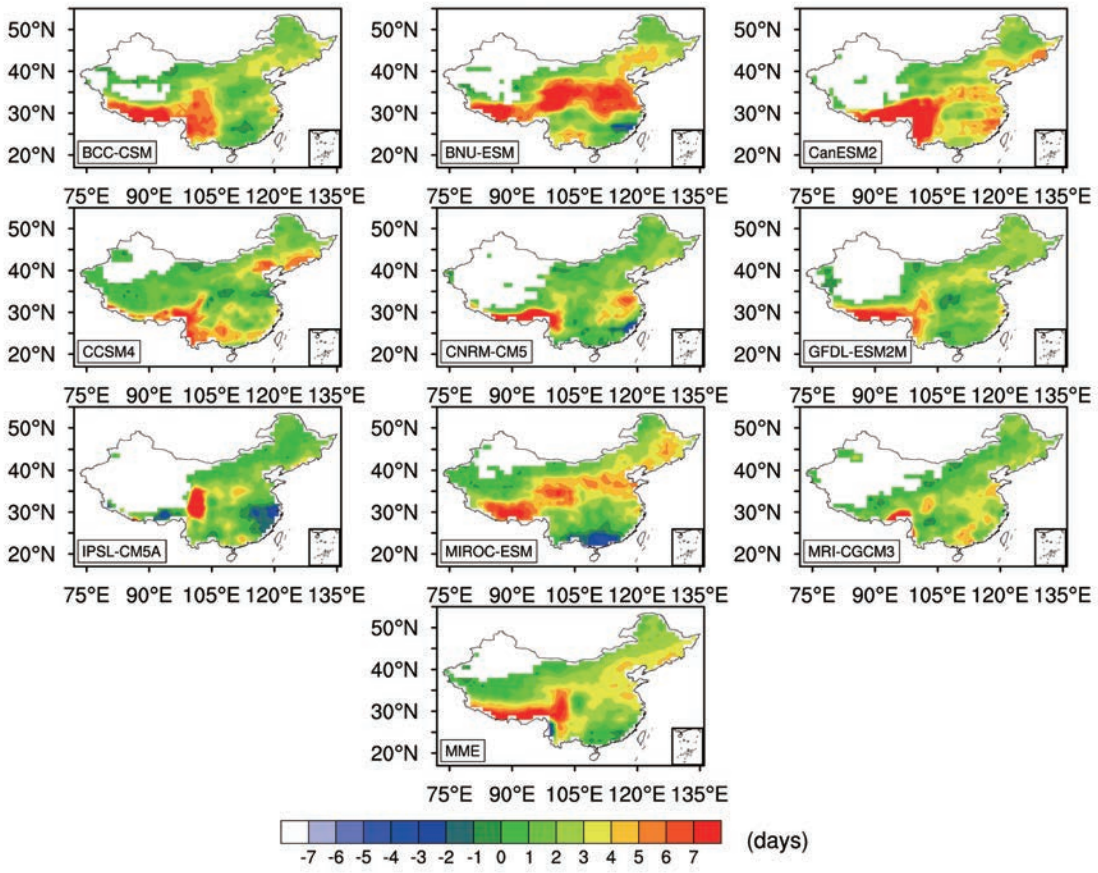

Fig. 10. The same as Fig. 9, but for R20 index.

For example, for TX90P, IPSL-CM5A and MIROC-ESM show a larger amplitude of increase compared to the other models under the three RCPs, with the northeast and center of China having a more significant increase (not shown). The change in R20 index is small and does not show a large spatial difference, although the amplitude in the area of the Bohai Sea is projected to grow as CO_2 emissions grow (see Fig. 10). The majority of the models reflect the pattern of a small amplitude of increase for P95T index in the north of Northeast China and in South China, and the changes in the area of the Bohai Sea are similar to those of the R20 index (not shown).

4. Summary and discussion

Extreme climate events have a serious impact on human society, the economy, and ecosystems. Thus, to be able to cope with climate change is of great concern. Based on CMIP5 results and observations, the spatial mean and changes in historical extreme climate over China have been analyzed in this paper, and then the projection of extreme temperature and precipitation indices under future RCP scenarios have also been investigated.

The results show that the global coupled models have a certain ability to reproduce the mean extreme indices, though the performance differs among the models and various indices. Most of the models perform well in simulating the mean value of FD and TX90P, R20 and P95T. However, the models' skills in reproducing the mean value of SU and TN10P need to be improved. The coupled models are also able to simulate the temporal evolution reasonably. Under the background of global warming, the trends of the extreme indices in the China region are consistent with that at the global scale; the model results reflect the decreasing trend of FD and TN10P and the increasing trend of SU and TX90P, but underestimate the magnitude of the FD trend while overestimating that of TX90P. Most of the models are able to generate trends of the same sign as in the observation for R20 and P95T, and have high spatial pattern correlation coefficients with observations; among all the indices in this study, FD, SU and P95T rank as the top three. To a certain extent, the models are able to provide the spatial difference between two mean states (1986–2006 and 1961–80) for the six indices. In particular, the models reproduce the spatial changes of the FD and SU indexes well, but most of the models need to improve their ability to reproduce the TN10P and TX90P spatial change patterns. The models are unable to reflect the uniform spatial change pattern for the R20 and P95T indexes.

In terms of future projection (2006–99), the FD and TN10P indexes show a decrease under RCP2.6, RCP4.5 and RCP8.5, while the SU, TX90P, R20 and P95T indices show an increase. Under the high emissions scenario of RCP8.5, the changes over the coming century based on the MME for

FD, SU, TN10P, TX90P, R20 and P95T are −46.9, 46.0, −27.1, 175.4, and 2.9 days, and 9.9%, respectively. The future spatial variation of the amplitude for each index is consistent with the emissions intensity. These results provide us with a useful and clear picture of future changes in climatic extremes over China, and to deal with the expected increases in extreme climate events, reductions of greenhouse gas emissions are crucial.

Compared to CMIP3 results (Jiang et al., 2012), the model skill in reflecting the mean FD and P95T value has been improved. Such improvements are reflected in the *E* for FD and P95T, which are much smaller in CMIP5 than in CMIP3. The future trend sign for FD and P95T is consistent with CMIP3 results. The linear trend magnitude under RCP2.6 is smaller than that of the B1 (lower emissions) scenario in CMIP3 results, but the linear trend magnitude under RCP8.5 is larger than that of the A2 (higher emissions) scenario.

Despite extreme climate events being shorter in duration and smaller in terms of their spatial scale, it is clear that global coupled climate models are able to basically capture their statistical characteristics. However, even though the historical and future model experiments are run under the standard framework supplied by CMIP5, large differences among the model results are still apparent, possibly as a result of individual features of the models themselves. For instance, the complexities of dynamic frameworks and physical process parameterizations of models; the different simulated climate sensitivities to climate forcings, such as changes in CO_2 or aerosol concentrations; or even the different ocean heat uptake efficiencies in the models. Therefore, great uncertainty still exists with respect to projecting extreme climate events in the future. However, by improving the parameterizations of physical processes in models, or working towards performing dynamic downscaling with more confidence, or by carrying out further ensemble simulations, we have the potential to reduce this uncertainty and improve the future projection of extreme climate events.

Acknowledgements. This work was funded by the National Key Program for Global Change Research of China (Grant No. 2010CB950500), the General Project of the National Natural Science Foundation of China (Grant No. 41275108), and the National High Technology Research and Development Program of China (Grant No. 2010AA012305).

REFERENCES

Alexander, L. V., and Coauthors, 2006: Global observed changes in daily climate extremes of temperature and precipitation. *J. Geophys. Res.*, **111**, D05109, doi: 10.1029/2005JD006290.

Chen, H. S., S. D. Fan, and X. H. Zhang, 2009: Seasonal differences of variation characteristics of extreme precipitation events over China in the last 50 years. *Transactions of Atmospheric Sciences*, **32**, 744–751.

Collins, M., S. F. B. Tett, and C. Cooper, 2001: The internal climate variability of HadCM3, a version of the Hadley Centre coupled model without flux adjustments. *Climate Dyn.*, **17**, 61–81.

Dunne, J. P., and Coauthors, 2012: GFDL's ESM2 global coupled climate-carbon Earth system models. Part I: Physical formulation and baseline simulation characteristics. *J. Climate*, **25**, 6646–6665.

Flato, G. M., G. J. Boer, W. G. Lee, N. A. McFarlane, D. Ramsden, M. C. Reader, and A. J. Weaver, 2000: The Canadian centre for climate modelling and analysis global coupled model and its climate. *Climate Dyn.*, **16**, 451–467.

Gao, X. J., Z. C. Zhao, and G. Filippo, 2002: Changes of extreme events in regional climate simulations over East Asia. *Adv. Atmos. Sci.*, **19**, 927–942.

Gent, P. R., and Coauthors, 2011: The community climate system model version 4. *J. Climate*, **24**, 4973–4991.

Gillett, N., V. Arora, G. Flato, J. Scinocca, and K. von Salzen, 2012: Improved constraints on 21st-century warming derived using 160 years of temperature observations. *Geophys. Res. Lett.*, **39**, L01704, doi: 10.1029/2011GL050226.

Hansen, J., and Coauthors, 1983: Efficient three-dimensional global models for climate studies: Models I and II. *Mon. Wea. Rev.*, **111**, 609–662.

Jiang, Z. H., Y. G. Ding, and Q. P. Tu, 1999: Interdecadal spatial structure and evolution of extreme temperatures in winter and summer over china during the past 50 years. *Quarterly Journal of Applied Meteorlolgys*, **10**, 97–103. (in Chinese)

Jiang, D. B., H. J. Wang, and X. Lang, 2004: Multimodel ensemble predication for climate change trend of China under A2 Scenario. *Chinese Journal of Geophyscics*, **47**, 776–784. (in Chinese)

Jiang, Z. H., Y. G. Ding, and W. L. Chen, 2007: Projection of precipitation extremes for the 21st Century over China. *Advances in Climate Change Research*, **3**, 202–207.

Jiang, Z. H., W. L. Chen, J. Song, and J. Wang, 2009: Projection and evaluation of the precipitation extremes indices over China based on seven IPCC AR4 coupled climate models. *Chinese J. Atmos. Sci.*, **33**, 109–120. (in Chinese)

Jiang, Z. H., J. Song, L. Li, W. L. Chen, Z. F. Wang, and J. Wang, 2012: Extreme climate events in China: IPCC-AR4 model evaluation and projection. *Climatic Change*, **110**, 385–401.

Karl, T. R., N. Nicholls, and A. Ghazi, 1999: Clivar/GCOS/WMO Workshop on Indices and Indicators for Climate Extremes Workshop Summary. *Climatic Change*, **42**, 3–7.

Kendall, M. G., 1948: *Rank Correlation Methods*. Charles Griffen and Company, 160 pp.

Lang, X., and Y. Sui, 2013: Changes in mean and extreme climates over China with a 2° global warming. *Chinese Science Bulletin*, **58**(12), 1453–1461.

Mann, H. B., 1945: Nonparametric tests against trend. *Econometrica: Journal of the Econometric Society*, **13**, 245–259.

Marti, O., and Coauthors, 2010: Key features of the IPSL ocean atmosphere model and its sensitivity to atmospheric resolution. *Climate Dyn.*, **34**, 1–26.

Meehl, G. A., T. Karl, and D. R. Easterling, 2000: An introduction to trends in extreme weather and climate events: observations, socioeconomic impacts, terrestrial ecological impacts, and model projections. *Bull. Amer. Meteor. Soc.*, **81**, 413–416.

Ren, G. Y., G. L. Feng, and Z. W. Yan, 2010: Progresses in observation studies of climate extremes and changes in mainland China. *Climatic and Environmental Research*, **15**, 337–353. (in Chinese)

Sillmann, J., V. V. Kharin, X. Zhang, F. W. Zwiers, and D.

Bronaugh, 2013a: Climate extremes indices in the CMIP5 multimodel ensemble: Part 1. Model evaluation in the present climate. *J. Geophys. Res.*, **118**, 1716–1733.

Sillmann, J., V. V. Kharin, F. W. Zwiers, and D. Bronaugh, 2013b: Climate extremes indices in the CMIP5 multimodel ensemble: Part 2. Future climate projections. *J. Geophys. Res.*, **118**, 2473–2493.

Voldoire, A., and Coauthors, 2011: The CNRM-CM5. 1 global climate model: Description and basic evaluation. *Climate Dyn.*, **40**, 2091–2121.

Watanabe, S., and Coauthors, 2011: MIROC-ESM: Model description and basic results of CMIP5–20c3m experiments. *Geoscientific Model Development Discussions*, **4**, 1063–1128.

Wang, H. J., and Coauthors, 2012: Extreme climate in China: Facts, simulation and projection. *Meteorologische Zeitschrift*, **21**, 279–304.

Wu, Q. Z., J. M. Feng, W. J. Dong, L. N. Wang, D. Y. Ji, and H. Q. Cheng, 2013: Introduction of the CMIP5 Experiments Carried out by BNU-ESM. *Advances in Climate Change Research*, **9**(4), 291–294. (in Chinese)

Wu, T., and Coauthors, 2010: The Beijing Climate Center atmospheric general circulation model: Description and its performance for the present-day climate. *Climate Dyn.*, **34**, 149–150.

Xie, P., M. Chen, S. Yang, A. Yatagai, T. Hayasaka, Y. Fukushima, and C. Liu, 2007: A gauge-based analysis of daily precipitation over East Asia. *Journal of Hydrometeorology*, **8**, 607–626.

Xu, Y., X. J. Gao, Y. Shen, C. H. Xu, Y. Shi, and F. Giorgi, 2009: A daily temperature dataset over China and its application in validating a RCM simulation. *Adv. Atmos. Sci.*, **26**, 763–772, doi: 10.1007/s00376-009-9029-z.

Yan, Z. W., and C. Yang, 2000: Geographic patterns of extreme climate changes in China during 1951–1997. *Climatic and Environmental Research*, **5**, 267–272. (in Chinese)

Yukimoto, S., and A. Noda, 2002: Improvements of the Meteorological Research Institute Global Ocean-atmosphere Coupled GCM (MRI-CGCM2) and its climate sensitivity. National Institute for Environmental Studies, Tsukuba, Japan, 37–44. [Available online at http：//160.202.2.12/Dep/cl/cl4/publications/yukimoto_CGER2002.pdf.]

Zhai, P. M., and X. H. Pan, 2003: Trends in temperature extremes during 1951–1999 in China. *Geophys. Res. Lett.*, **30**, doi: 10.1029/2003GL018004.

Zhai, P. M., X. B. Zhang, H. Wan, and X. H. Pan, 2005: Trends in total precipitation and frequency of daily precipitation extremes over China. *J. Climate*, **18**, 1096–1108.

Zhai, P., A. Sun, F. Ren, X. Liu, B. Gao, and Q. Zhang, 1999: Changes of climate extremes in China. *Climate Change*, **42**, 203–218.

Zhang, Y., Y.-L. Xu, W.-J. Dong, and L. Cao, 2007: A preliminary analysis of distribution characteristics of maximum and minimum temperature and diurnal temperature range changes over China under SRES B2 scenario. *Chinese Journal of Geophysics*, **50**, 714–723. (in Chinese)